

A Low-Wear Onload Tap Changer Diverter Switch for Frequent Voltage Control on Distribution Networks

Daniel J. Rogers, *Member, IEEE*, Tim C. Green, *Senior Member, IEEE*, and Richard W. Silversides, *Member, IEEE*

Abstract—This paper presents a fast mechanical diverter switch design suitable for new “arcless” hybrid onload tap-changing systems. In such systems, arcing at contact separation and contact closure is almost completely eliminated by the inclusion of alternate current paths incorporating semiconductor devices. This allows the use of compact, air-insulated mechanical contacts that do not need to withstand significant arc erosion or provide arc quenching. As a result, the moving mass and the drive system for the switch may be dramatically reduced in size, leading to low inertia of the moving parts and resulting in very rapid operation times. An integrated, high-torque, low-mass permanent-magnet actuator is presented that provides detent (unpowered) contact force coupled with a cantilever spring contact system sized for an 11-kV 2-MVA onload tap changer. The design delivers operation times of under 20 ms and is capable of sustaining more than 10^6 operations. The complete design is experimentally verified under representative electrical conditions, and contact wear levels comparable to pure mechanical (zero current) operation are demonstrated.

Index Terms—Arc discharges, contacts, permanent-magnet machines, power distribution, switches, switchgear, voltage control.

I. INTRODUCTION

THE HYBRID onload tap changer (OLTC) combines mechanical switching elements and power semiconductor devices to provide a balance in performance across a number of metrics when compared to purely mechanical (or “classic”) OLTCs and OLTCs based upon power semiconductor devices alone. Hybrid OLTCs typically employ mechanical contacts to carry the load current when operating in the steady state (i.e., while not performing a tap change), resulting in very low conduction losses and a high tolerance of network fault currents. When a tap change is required, the hybrid OLTC employs a low-rated power-electronic circuit to divert current out of the main current path and into an alternate thyristor-based path which is then used to commutate the current into another transformer tap. Once the current has been fully transferred to the

Manuscript received April 15, 2013; revised June 28, 2013; accepted July 01, 2013. Date of publication August 01, 2013; date of current version March 20, 2014. This work was supported by a UK EPSRC Doctoral Training Award and was conducted partly within the Supergen FlexNet programme. Paper no. TPWRD-00441-2013.

D. J. Rogers is with the Institute of Energy, School of Engineering, Cardiff University, Cardiff CF24 3AA, U.K. (e-mail: RogersDJ@cardiff.ac.uk).

T. C. Green and R. W. Silversides are with the Electrical and Electronic Engineering Department, Imperial College London, London SW7 2AZ, U.K. (e-mail: t.green@imperial.ac.uk; r.silversides@imperial.ac.uk).

Color versions of one or more of the figures in this paper are available online at <http://ieeexplore.ieee.org>.

Digital Object Identifier 10.1109/TPWRD.2013.2272335

new tap, a mechanical switch is closed to bypass the thyristors and return the system to steady-state operation. This process is illustrated in Fig. 1 for an *active-shunt*-type hybrid OLTC [1].

An important future hybrid-OLTC application will be in the support of high levels of electric-vehicle (EV) charging on the distribution network, perhaps coupled with a high penetration of intermittent distributed generation [e.g., photovoltaics (PV)]. Both EV charging and PV generation can lead to large and frequent variations in feeder current, due to highly correlated EV charging profiles and/or local cloud shadowing of many PV installations [2]. Due to the low X/R ratio of low-voltage (LV) lines, voltage control based on reactive compensation is not practical, and direct voltage control in the form of OLTCs will be necessary to maintain supply within voltage limits without resorting to comparatively expensive cable upgrades. In all cases, the speed of response, service interval, lifetime, robustness, and power losses are key measures of OLTC performance.

Table I summarizes the attributes of classic, semiconductor-only, and hybrid OLTC technologies. In general, the semiconductor-only OLTC may operate extremely quickly and incurs no wear penalty per operation; however, as one or more semiconductor devices must carry the load current continuously, the system is vulnerable to and must be dimensioned to cope with network fault events (i.e., overcurrent) and incurs relatively high operating power loss. The classic OLTC relies on mechanical contact movement to perform tap changes and is therefore relatively slow; however, due to the very low path resistance, the losses are negligible and the system is robust against network faults. A major factor contributing to the limited lifetime of the classic OLTC is the heavy arcing that inevitably occurs at every tap change operation: this places a fundamental limit on the number of operations that the system may perform before requiring replacement of the contacts.

The hybrid OLTC may be expected to deliver much greater contact lifetime when compared to the classic OLTC because contact arcing is eliminated by the operation of an auxiliary circuit that removes current from the mechanical contacts before they are opened (this process is explored in detail in [1]). An additional benefit of the elimination of arcing is an increase in operating speed relative to the classic OLTC. This is a result of a reduction in the contact mass required in the switch due to the elimination of arc-induced erosion of the contact surfaces. Since contact erosion is no longer a concern, the chief design constraint dictating contact size becomes current handling capability and so the switch may be made smaller and lighter. Furthermore, as no arc is drawn at contact separation, the arc quenching properties of oil or SF_6 are not required. Air- or CF_3I -insulated diverter switches therefore become possible

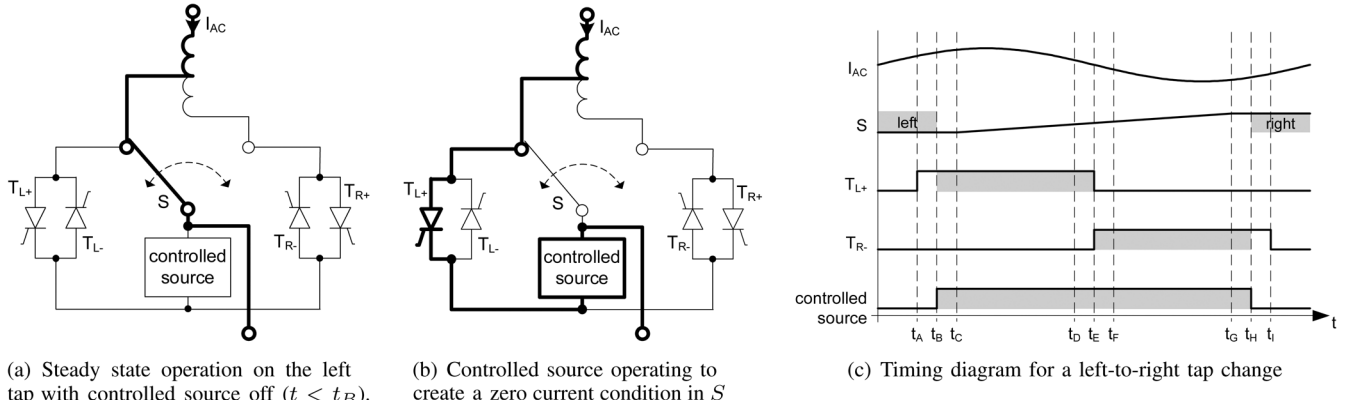


Fig. 1. Tap change timing diagram and example current paths for a single phase of an active-shunt OLTC. (a) and (b) illustrate the diverter subcircuit only and do not show the selector circuitry. See [1] for a full set of current paths and a timing diagram including selector switch operation. (c) S low indicates the switch is in the left position, S high that the switch is in the right position, intermediate values represent switch movement (i.e., an open condition). High T_{L+} or T_{L-} indicates that trigger current is applied. A high level for the controlled source indicates that it is operating to ensure zero current conditions in the switch. Bold lines and shaded regions indicate device conduction of I_{AC} . Note that the thyristors are only required to block the intertap voltage (which will be of the order of 1% of the rated voltage of the system) and only carry the load current for the short duration of the tap change.

TABLE I
COMPARISON OF OLTC TECHNOLOGIES

	Classic	Semiconductor	Hybrid
Tap-to-tap time	3 s [4]	100 μ s	20-50 ms [5]
Operation count	3×10^5 [6]	extremely high ¹	$> 10^7$ [1]
Fault robustness	very high	low ²	high ³
Capital cost	low	high ⁴	low
Conduction losses	negligible ⁵	high ⁶	negligible ⁵

¹ limited only by long-term reliability of the semiconductor devices;

² fault robustness is determined largely by the chosen over-dimensioning of the semiconductor devices (devices will typically need to tolerate at least 10-p.u. current for 100 ms); ³ semiconductors in hybrid OLTCs typically must withstand fault current for no longer than 20 ms (see Section II); ⁴ a large number of high-power semiconductor devices is a major cost; ⁵ mechanical contact conduction losses only; ⁶ for a thyristor diverter rated at 2 MVA, total junction losses will be in the order of 2 kW.

under appropriate hybrid schemes. A gas-insulated system will experience minimal mechanical drag and may be expected to achieve the highest operation speeds, while the use of alternate gases will reduce environmental harm arising from the very high global warming potential of SF₆ [3].

II. FAST DIVERTER SWITCH DESIGN

The minimum time required to perform a single tap change under a hybrid OLTC scheme is fundamentally limited by the use of thyristors in the diverter subcircuit to handle the commutation between taps; every tap change operation must cover a zero crossing of the load current in order to effect the handover from one side of the diverter circuit to the other. This means that a hybrid OLTC can theoretically provide voltage corrections within 10 ms (assuming 50-Hz line frequency) of receiving a command signal, allowing changes in feeder current (and, therefore, feeder voltage) to be tracked accurately. In order to correct large disturbances, additional tap changes may be performed with similar half-cycle delays.

A fast diverter switch is desirable under hybrid schemes for two reasons. First, the time required by the system from receiving a tap change command to carrying out the tap change operation is directly dependent on the time required to open the

closed diverter switch. A slow diverter switch would effectively incur a latency penalty; the system must wait until the diverter switch is fully open before performing a current handover at the next load current zero crossing. In order to minimize this “first tap latency,” it is important to have a fast-acting diverter switch.

Second, under network fault conditions, fast switches will offer greater protection to the semiconductor devices used within the OLTC. During a tap change operation, the load current through the selector and diverter is carried by the semiconductor devices (thyristors and controlled source components). If a fault were to occur in this period, then any resulting fault current would flow through these potentially sensitive devices. However, the fault current can be moved rapidly out of the semiconductor device path with the closure of the selector and diverter switches. If a fault current were to be detected, the diverter and selector switches would be triggered to close immediately and the semiconductor devices must only survive the fault current for the period of time required for the switches to reach the closed state. Faster mechanical switches directly translate into relaxed requirements regarding the overcurrent tolerance of the semiconductor devices.

Note that the sequential tap change speed (e.g., moving from tap 1 \rightarrow 2 \rightarrow 3 without pause) is limited by the speed of the *selector* switches, not the diverter switch. When performing sequential tap changes, the diverter switch may be held in an off state and the tapping performed using the diverter thyristor pairs alone: diverter switch speed is therefore not a limiting factor in this case.

In order to investigate the feasibility of compact, high-speed, air-insulated mechanical switches for OLTC applications, the authors have sought to construct a proof-of-concept device to fulfill the key criteria of high-speed operation and very high operation count capability.

A. Basic Design

The switch design presented in this paper is intended for an air-insulated 11-kV 2-MVA star-connected OLTC appli-

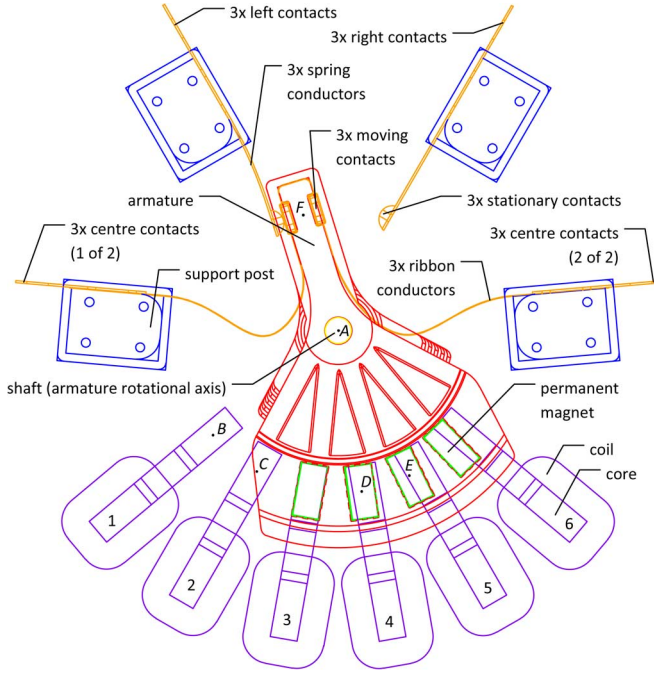


Fig. 2. CAD wireframe rendering of the switch. Top view of the switch in the left-on position showing the deflection of the cantilever contact and the resulting displacement of the magnets from the minimum energy position. See Fig. 7 for an alternative view of the switch. The pole and magnet radii are equal ($AB = AD = 60$ mm) and the contact radius $AF = 45$ mm. The pole pitch angle is $BAC = 20^\circ$ and in this diagram, a magnet pitch angle of $DAE = 18^\circ$ is illustrated (the selection of magnet pitch is discussed in Section II-B).

cation (nominal phase current of 100 A). The switch is an integrated three-phase, double-throw design driven by a permanent-magnet actuator and uses cantilever-spring contacts. This type of design has low mechanical complexity and low inertia, allowing for reliability at high operation counts and very high actuation speed. A particular advantage of the double-throw design is that the switch is guaranteed to pass through the off state during operation (break before make), a fundamental behavior required by all OLTC schemes. The basic mechanical design of the switch is illustrated in Fig. 2. The important design decisions and tradeoffs are discussed in the following sections.

B. Magnetic Design

A principle design constraint is that the switch should remain in a stable state should a failure in the actuation system (power supply, drive electronics, sensing systems, etc.) cause the actuator to become disabled. This will enable the OLTC to continue functioning on the current tap but without the ability to perform further tap change operations. Thus, a detent torque should be provided in the closed states independent of any external power supply. In order to meet the speed-of-operation target, a high torque-to-inertia ratio is also desirable. A permanent-magnet actuator design employing high-strength rare-earth magnets can meet both of these criteria.

Some aspects of the magnetic design are visible in Fig. 2. A set of six c-cores are regularly spaced at angles of 20° about the central axis of the switch. The cores provide a low reluctance

path for the flux driven by the coil wound around the rear section. The core flux interacts with the field created by a set of four permanent magnets, also regularly spaced and fixed into the armature that passes through the gap in the cores, and oriented in alternating magnetic direction parallel to the armature central axis. In the following discussion the c-cores plus coils are referred to as “poles” and the armature permanent magnets are referred to as “magnets.”

When the poles are appropriately energized, it is possible to generate motive torques of large magnitude in either direction. The armature is not used as a flux path and may therefore be constructed of a lightweight plastic, resulting in a low inertia design. Crucially, when the poles are unenergized (i.e., zero current is flowing in the coils), an attractive force between magnets and poles will still be present, allowing a detent torque to be maintained without external power. This is often a special requirement for electromagnetic actuators for electrical switching systems, for example, [7].

A tradeoff is evident in the choice of the magnet pitch angle. A magnet pitch that is equal to the pole pitch produces the greatest peak contact force in the *unenergized* state since each magnet may simultaneously be positioned in a high-force state when displaced from the nearest pole gap. However, this pitch produces the maximum torque ripple in the *energized* state since no torque may be produced when every magnet is positioned centrally in a pole gap. Conversely, a three-quarter magnet-pole pitch (i.e., where $\angle DAE = (3/4)\angle BAC$) produces minimum torque ripple in the energized state but very little static contact force may be generated in the unenergized state.

A conceptually simple scheme to generate high actuation torque in the energized state is to set the magnetization direction of each pole so that the pole closest to any given magnet exerts an attractive force if the magnet lies behind the pole in the desired direction of travel. Similarly, if the closest magnet lies ahead of the pole, the pole magnetization direction is set such that it repels the magnet from the gap. This procedure is repeated for each pole and determines the coil drive current pattern to provide high actuation speed while requiring a low number of drive switching transitions per actuation. A result of this simple algorithm (coupled with the alternating magnet magnetization direction) is that the *second*-closest pole to any given magnet is magnetized in a direction such that it constructively adds to the force in the desired direction of travel. This algorithm is valid for any magnet-pole pitch.

Fig. 3 presents the results of multiple static 2-D finite-element simulations representing the magnetic design of Fig. 2 at various armature displacements and for varying magnet pitch angles. The relationship between static contact force in the unenergized state and torque ripple in the energized state is clearly visible. This 2-D analysis [8] models a flattened version of the actual system: the depth of the model was set equal to that used in the design (20 mm) but the nonparallel nature of the magnets and poles was not modelled (i.e., the magnets and poles were considered to be parallel through their depth). A 3-D finite-element simulation would capture the curvature of the real system, and enable the modelling of the out-of-plane nature of the c-core magnetic circuit but at the cost of much greater computational complexity. As discussed in Section IV-D, good agreement was

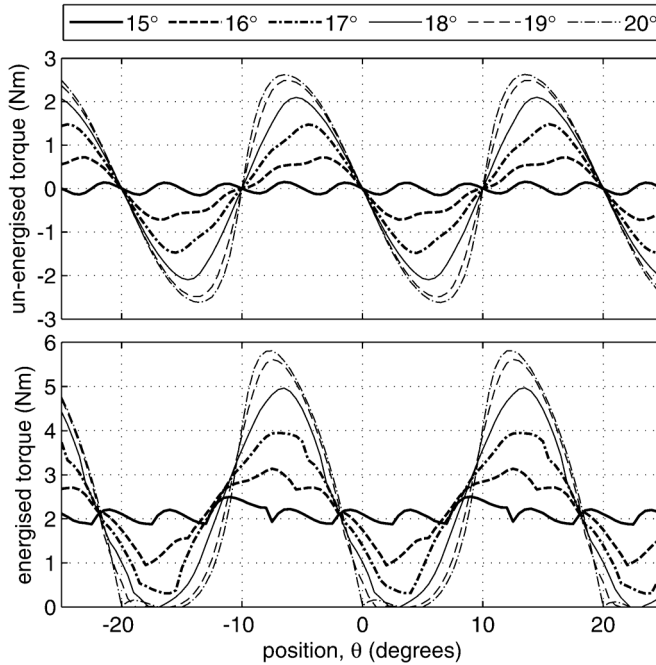


Fig. 3. Torque-position relationships derived from a finite-element model for varying magnet pitch angles using FEMM v4.2 [9]. Permanent-magnet type is SmCo27, and poles operated to a saturation flux density of approximately 1.2 T.

observed between the results generated by the prototype device and results from simulation models based on the torque-position data generated by the 2-D finite-element model (i.e., Fig. 3). Given the modelling uncertainties elsewhere in the system (particularly the behavior of the cantilever spring contacts), it is unlikely that a 3-D finite element would provide significantly improved simulation accuracy.

For all pitch angles other than 15°, the unenergized plot of Fig. 3 exhibits stable equilibrium points (where $T = 0$ and $dT/d\theta < 0$) corresponding to the positions in which the armature should remain without power: Left-on (-20°), center-off (0°), and right-on (20°). In the left and right positions, the contact springs will exert a counter torque that acts to push the armature toward the center of the torque-position graph. A new equilibrium point will be found where the combined spring torque exactly balances the magnetic torque acting on the armature. It is intended that the spring arrangement be adjusted so that the maximum contact force be exerted by the magnetic system at the spring-magnet equilibrium point.

An equal magnet-pole pitch (BAC = DAE = 20° in Fig. 2) is unique for two reasons. First, the pole-drive pattern required to produce the maximum torque is such that each coil requires identical current *magnitude* but with alternating current *direction*. This means that the coils may be connected in anti-series (i.e., coil 1 is in the clockwise direction, coil 2 is in the anti-clockwise direction, coil 3 is in the clockwise direction, etc.) and driven from a single electrical source. This simplifies the power-electronic drive circuit considerably when compared to any unequal magnet-pole pitch, which would require the use of six separate drive circuits for each coil in order to maximize the generated torque. Second, for an equal magnet-pole pitch, the stable equilibrium points of the unenergized plot coincide with the zero-torque points of the energized plot of Fig. 3. This

occurs when each magnet directly occupies a pole gap and is an undesirable characteristic of equal magnet-pole pitch: if the system were to come to a standstill in the center position (0°) (where no spring torque is present), the actuation mechanism may be incapable of subsequently dislodging the armature (this situation could arise due to a power failure midactuation cycle for example). Such a situation does not exist for an unequal magnet-pole pitch.

C. Static Contact Force and Contact Temperature Rise

One criteria for selecting magnet pitch is the requirement to provide a minimum static contact force to avoid excessive contact temperature rise under worst-case operating conditions. The peak temperature T (the supertemperature) in a homogeneous electrical contact subject to a current I and an applied force F_c may be estimated by solving a pair of coupled equations determining contact resistance R [10], [11]. The first equation relates the resistance R of a contact to the applied contact force F_c , including the effect of supertemperature T

$$R = \frac{\rho}{2} (1 + \nu(T - T_0)) \sqrt{\frac{\eta\pi H}{F_c}} \quad (1)$$

where ρ is the electrical resistivity and λ is the thermal conductivity of the contact material at bulk contact temperature T_0 , ν represents the change in electrical resistivity conductivity with temperature. H is the yield strength of the contact material and η is a constant of order unity which depends on contact material and shape. The second equation relates the supertemperature to the voltage drop across the contact; this voltage is a product of the effective contact resistance R and the contact load current I

$$IR = 8\rho\lambda \left(T - T_0 - \frac{\nu + \beta}{2} (T^2 - T_0^2) + \frac{\nu\beta}{3} (T^3 - T_0^3) \right) \quad (2)$$

where β represents the change in thermal conductivity of the contact material with temperature. Equations (1) and (2) may be solved to find the contact temperature rise $\Delta T = T - T_0$ at a given contact force and current, as shown in Fig. 4. The contact temperature rise is minimal at the nominal operating current of 100 A even at forces as low as 2 N. However, for a 10-p.u. fault current, the temperature rise may approach several tens of degrees even at quite large contact forces. It is desirable to limit the peak contact temperature to well below the softening point of copper (roughly 180 °C [10]) in order to limit thermal processes which may damage the mechanical properties of the cantilever spring contacts. A contact force of 10 N is sufficient to limit the temperature rise at 10-p.u. current to under 40 °C. Note that contact resistance and, hence, temperature rise is dependent to some degree on contact geometry and contact material and this calculation serves only to demonstrate the order of magnitude of contact force that is required to adequately limit temperature rise. Particularly, the *bulk* resistance of the contacts, coupled with the thermal mass and the limited dissipation capability of the contact system, imply that T_0 will be significantly greater than ambient, both reducing the allowed ΔT and limiting the length of time over which a fault current may be applied to a few hundred milliseconds.

A particular static contact force is achieved by setting an equilibrium contact point such that the permanent magnets are dis-

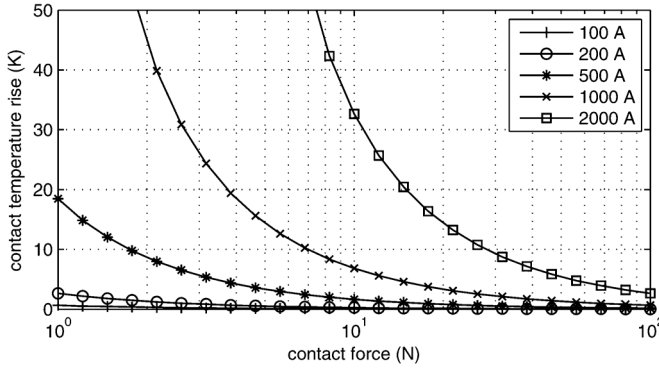


Fig. 4. Contact temperature rise against contact force for copper contacts at various currents. The bulk contact temperature is $T_0 = 100^\circ\text{C}$ and $\eta = 1$.

placed some distance from their minimum energy position by the action of cantilever contacts. The equilibrium contact point is formed when the spring torque generated by the cantilever contacts exactly balances the magnetic torque of the actuator. If r_c is the contact radius (see Fig. 2, $r_c = AF = 45$ mm in this design), the contact force per phase may be calculated from

$$F_c = \frac{T_m}{3r_c} \quad (3)$$

for a magnet pitch angle of 18° , the peak static magnetic torque from Fig. 3 is 2.08 Nm, giving $F_c = 15.4$ N. Note that (3) contains a factor of $1/3$ due to the use of three cantilever springs.

The design of the cantilever contacts should be such that the equilibrium point is at the maximum static magnetic torque position. From the desired contact deflection w and a known peak static contact force, the required cantilever thickness may be estimated from the Euler–Bernoulli beam equation [12] as

$$b = L \sqrt{\frac{4F_c}{Ehw}} \quad (4)$$

where E is the Young's modulus of the cantilever material and L and h are the length and height of the cantilever, respectively (33 and 19 mm in this design). For this design, the springs were constructed from a beryllium copper strip to provide high electrical conductivity, backed by a carbon (spring) steel strip to provide the majority of the spring force and the required mechanical robustness over many operating cycles.

III. SWITCH MODELING

The torque-position information of Fig. 3 may be used as an input to a lumped-mass mechanical model representing the mechanical system of Fig. 2, described by

$$\ddot{\theta} = \frac{1}{J} (T_m(\theta) + r_c F_t(r_c \theta)) \quad (5)$$

where $T_m(\theta)$ describes the kinematic torque-position relationship of Fig. 3 and $F_t(x)$ describes the forces delivered by the cantilever spring contacts. The contact linear position x_c is found from the rotational position of the armature θ via the contact radius r_c . The angular velocity of the armature

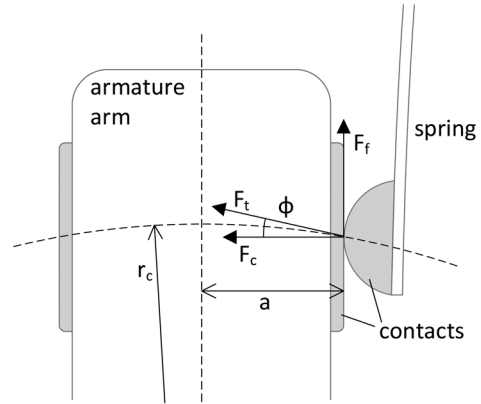


Fig. 5. Contact forces at switch closure, $F_f = \text{sgn}(\omega)\mu F_c$ is the frictional force between contacts which always opposes the direction of sliding. $a = 8$ mm.

is $\omega = \dot{\theta}$. The moment of inertia of the armature assembly (armature piece, magnets and contacts) was calculated using CAD software as $J = 4.41 \text{ kg cm}^2$.

In this model the cantilever spring contacts are considered massless (i.e., they apply no inertial forces to the armature); only spring forces are modelled. The springs exert an accelerating force at the start of the movement and a decelerating force at the end of the movement such that

$$F_c = \begin{cases} 3kr_c(\theta_c - \theta), & \text{for } \theta \leq -\theta_c \\ -3kr_c(\theta - \theta_c), & \text{for } \theta \geq \theta_c \\ 0, & \text{otherwise} \end{cases} \quad (6)$$

where θ_c is the angle at which the armature makes contact with the undeflected spring (11.5° in this design) and $k = Eb^3h/4L^3$ is the spring constant of each cantilever spring. The necessary spring deflection w is simply the linear distance between the peak static magnetic torque position denoted θ_m and the undeflected spring position

$$w = r_c(\theta_m - \theta_c) \quad (7)$$

from this equation, and the spring thickness may be chosen according to (4) such that the peak static contact force is achieved.

Frictional forces between the contacts are considered as the only form of loss (damping) within the mechanical model. The resulting damping force tangent to the actuation arc (i.e., normal to the armature central axis) may be calculated for the right-hand contact with reference to Fig. 5 as follows:

$$\phi = \arcsin\left(\frac{a}{r_c}\right), \quad F_t = F_c \cos(\phi) + F_f \sin(\phi) \quad (8)$$

$$= F_c \left(\sqrt{1 - \frac{a^2}{r_c^2}} - \text{sgn}(\omega)\mu \frac{a}{r_c} \right) \quad (9)$$

where μ is the coefficient of friction between contacts (approximately equal to unity for clean homogenous copper contacts). Note that the verse (sign) of the frictional force always opposes the sliding motion of the contacts, hence the use of $\text{sgn}(\omega)$.

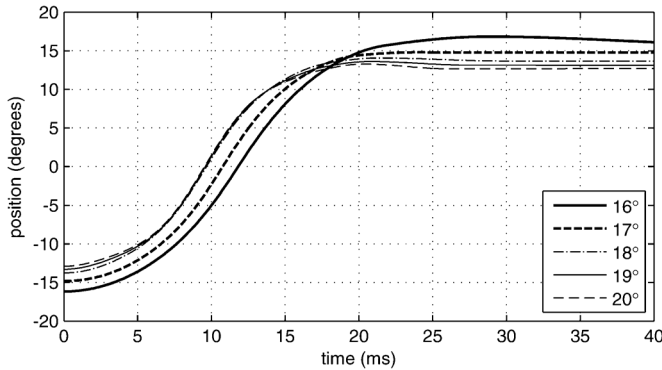


Fig. 6. Simulated actuation cycles for various magnet pitch angles. Poles energized at 10 ms, pole currents reversed at $0.03\theta_0$, poles de-energized at $0.97\theta_0$.

A. Control of Closing Velocity

The kinetic energy imparted to the armature during the actuation cycle will be dissipated in the contacts when the moving contact impacts the stationary contact after it has traversed the actuation angle. Ideally the impact velocity, and therefore impact energy, would be equal to zero in order to minimise mechanical wear of the contact surfaces and minimise impulse forces experienced by the armature assembly. This may be achieved by reversing the actuation torque (by reversing the direction of the coil currents) roughly mid-way through the actuation angle. In this way the armature is accelerated for the first phase of the actuation cycle and then decelerated for the remainder of the cycle. Once the armature has reached a position where the unenergized (static) magnetic torque is sufficient to maintain contact force at the new spring-magnet equilibrium point the drive currents may be entirely removed. The point at which actuation torque is first reversed and then finally removed depends upon the natural damping (frictional losses) of the system and the properties of the cantilever spring contacts.

B. Simulation Results

Sample actuation position-time profiles produced by the simulation model for different magnet pitch angles are shown in Fig. 6 (simulations performed in MATLAB Simulink). Due to the varying placement of the maximum static magnetic torque point with magnet pitch, the start and end positions for each pitch are different. For this reason, the start of the deceleration phase is set relative to the total range of motion (equal to $2\theta_0$, where θ_0 corresponds to the equilibrium point found when the static magnetic torque and the spring torque are equal). The 15° pitch provides virtually no static contact force and, thus, is considered unsuitable for the final system and is therefore not included in the simulation results.

The simulation results demonstrate the relative insensitivity of actuation time to magnet pitch, especially in the range $18\text{--}20^\circ$. If actuation time t_a is defined as the time between energizing the poles and the armature reaching θ_c , actuation in under one cycle of the mains waveform is possible (e.g., $t_a \approx 18$ ms for a spacing of $18\text{--}20^\circ$).

IV. EXPERIMENTAL RESULTS

A prototype diverter switch was constructed to verify the speed of operation and to test the operation count capability of the design. A further goal was to investigate the wear characteristics of relatively small, pure copper contacts subject to large conduction currents but small residual currents at the switch opening, consistent with the condition expected under a hybrid diverter scheme such as that described in [1]. The observations of Section II-B, regarding the advantages and disadvantages of equal magnet-pole pitch, lead to a design choice: equal magnet-pole pitch gives maximum static drive torque and a greatly simplified drive circuit arrangement, but there is the danger of the armature becoming stuck at the center-off stable equilibrium point. For the prototype switch, an equal magnet-pole pitch of 20° was chosen, partly to enable an investigation of the likelihood of becoming stuck in the center-off position during long-term operation and to achieve maximum static contact force in the left and right closed states. Individual drivers for each coil were constructed, but for the experimental results presented in this paper, the drivers were operated in unison to emulate an anti-series connection of coils driven from a single source.

A. Prototype Construction

The prototype switch (shown in Fig. 7) was constructed from a small number of large components: the armature, the top plate, the bottom plate, the contact pillars, and the support pillars. All but the support pillars were manufactured from nylon using the selective laser sintering (SLS) process. This is a rapid prototyping technique that creates 3-D objects from powder by melting successive layers of material to build up the structure. This allowed the complex shapes of the components to be created rapidly and at low cost.

The permanent magnets are SmCo26 $20 \times 10 \times 5$ mm magnetized across the shortest dimension and fitted in alternating magnetic orientation. The six cores were made from 0.05-mm tape-wound laminated silicon steel with 40 turns of 1-mm diameter copper wire. The springs were constructed from 0.75-mm beryllium-cobalt-copper alloy with a backing of 0.5-mm spring steel to give the required stiffness. The fixed and moving contact surfaces were made from pure copper.

B. Drive System and Control Scheme

Control of the switch was achieved using a simple 8-bit microcontroller to generate an independent current setting for each pole based on the rotational position of the armature. Independent metal-oxide semiconductor field-effect transistor (MOSFET) H-bridge circuits operating from a 60-V dc supply were used to drive a fully controllable current in the range ± 10 A in each core coil (the cores were found to saturate at approximately 8 A). The individual drivers were operated in anti-series unison for the reasons discussed previously. Current-mode hysteresis controllers implemented using analog components were used to ensure the system would respond quickly to changes in the current set points requested by the microcontroller. Position feedback of the armature was provided by an 11-bit optical absolute encoder attached to the shaft of the armature. Initiation of switching was controlled from a PC connected to

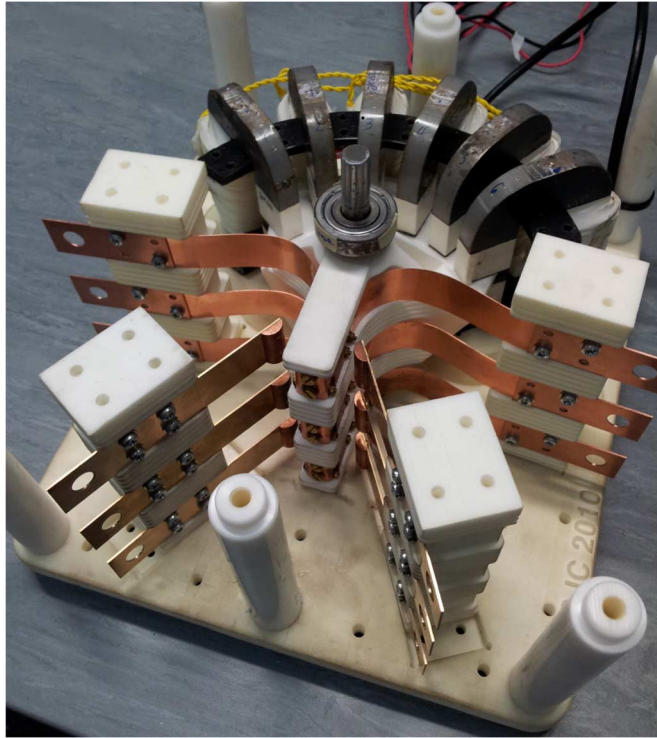


Fig. 7. Photograph of the prototype switch with the top plate removed. The bottom plate, armature, and contact pillars were constructed from nylon using the SLS technique. The armature is shown in the center-off position.

the microcontroller; this link was also used to supply data about the operation of the switch from the microcontroller to the PC.

Position control of the armature was handled directly by the microcontroller and was achieved by setting the pole current as described in Section II-B. A simple threshold-based algorithm was used to change the current in the poles when the armature reached the relevant positions. A recorded sequence from the prototype showing armature movement from -15° to 15° is given in Fig. 8. The operation is initiated at A by setting the current in the six poles to generate maximum positive torque. Due to the alternating permanent-magnet orientation, the current in poles 1, 3, and 5 is set to 7 A while the current in poles 2, 4, and 6 is set to -7 A. The armature accelerates away from the stable rest position. When the armature reaches 0° (B), the magnets are aligned with the cores and the current reference to the controller is reversed so that the armature will continue to accelerate towards the end of its travel. Note that the inductance of the pole circuit acts to limit the achievable dI/dt . At C, the current reference is reversed once more in order to generate negative torque so that the armature is decelerated to its end stop. When the contacts initially meet (D), the current in the coils is allowed to decay to zero. The armature continues to move due to its inertia and the attraction force between the permanent magnets and the de-energized poles. Some overshoot and oscillation of the armature after the pole current is reduced to zero is evident by the zero current segments between D and E (the armature reaches a maximum angle of 18° at E). Once these oscillations have decayed, the armature settles at a position of 15° .

It was observed that if the control algorithm was set up incorrectly (e.g., by setting the deceleration set point (C) too early

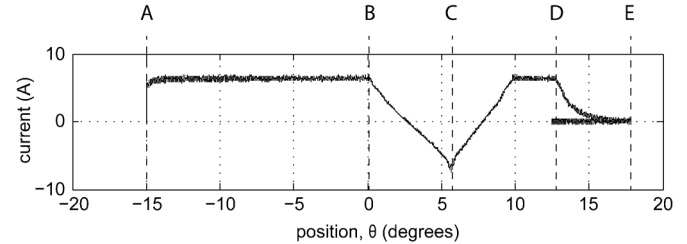


Fig. 8. Coil current recorded for pole 1 over a single actuation of the prototype from the left (-15°) to right (15°). The equal magnet-pole pitch of the prototype allowed the use of series-connected coils; therefore, the current flowing in the odd-numbered coils was identical and that in the even-numbered coils is negative to that shown here.

in the cycle), the armature could come to rest in the center-off position. Once in this position, it was impossible to dislodge the armature by applying current to the coils and an externally applied torque was required to place the armature in the left-on or right-on positions and allow continued operation. For a correctly tuned control algorithm, the armature was never observed to become stuck in center-off state (the inertia of the armature reliably carried it beyond this stable equilibrium position for every actuation in the trial run). This suggests that a production system may be able to reliably avoid becoming stuck in this position, although clearly this raises questions regarding the behavior of such a system when subject to, for example, unexpected power loss. If the (remote) possibility of becoming stuck under extreme conditions is unacceptable, the additional complexity inherent in choosing an unequal magnet-pole pitch or introducing a mechanical or magnetic biasing scheme capable of dislodging the armature from the center-off position may be unavoidable.

C. Electrical Contact Connections

The prototype diverter switch was constructed with three-phase contacts. This allowed three contact endurance tests to be carried out simultaneously. The three tests were designed to investigate contact wear in a high-speed diverter switch operating under a hybrid tap changer regime as follows.

- 1) A reference case in the form of a purely mechanical test, with no current flowing in the contacts.
- 2) A residual current break test with small dc current (500 mA) flowing in the contacts at contact separation. This is representative of the residual current generated by the hybrid diverter electronics described in [1].
- 3) A full-load current test with 100 A (ac rms) flowing in the contacts, but where the current is interrupted by an external device prior to contact separation. This test was designed to investigate the extent to which the heating effect of the load current affects contact wear.

None of the aforementioned cases involve the breaking of the full 100-A load by the diverter switch since this would incur heavy arcing leading to the destruction of the contacts in very few operations. No visible arcs were formed in any of the aforementioned tests; the residual currents and switch voltages were below that generally acknowledged to cause significant arcing between copper contacts [13]. “Prestrike” arcing at the contact closure can also not occur in any of these tests because the current is blocked by external means (thyristor pairs).

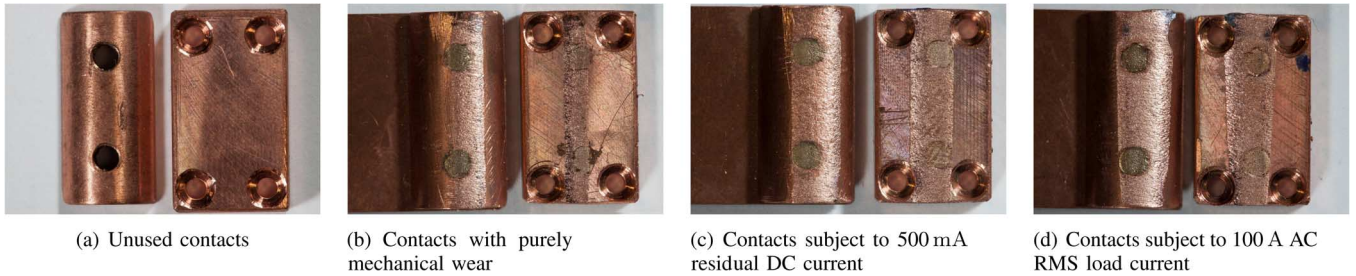
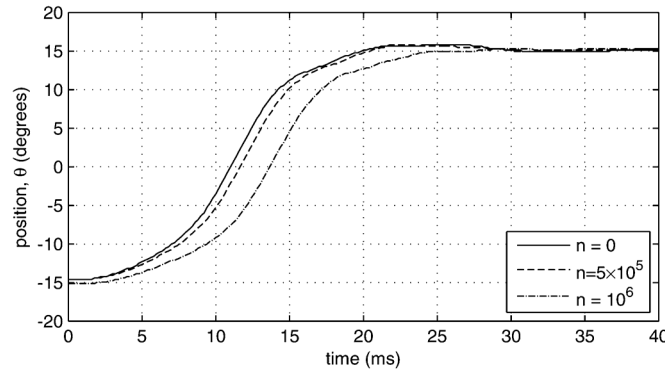
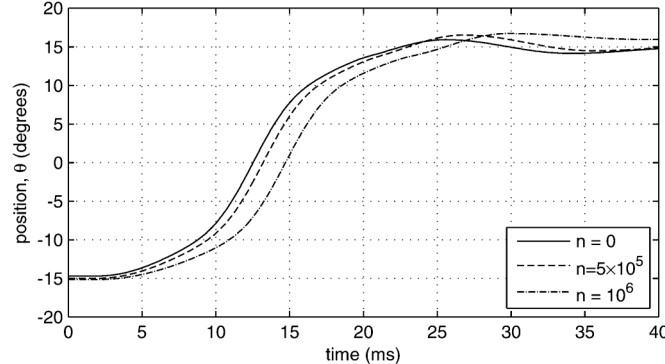


Fig. 9. Photographs of contacts after 10^6 operations. (a) Unused contacts. (b) Contacts with purely mechanical wear. (c) Contacts subject to 500 mA residual dc current. (d) Contacts subject to 100-A ac rms load current.



(a) Results recorded from the prototype diverter switch



(b) Simulation results for the diverter switch using the coefficients given in Table II.

Fig. 10. Comparison of the (a) recorded and (b) simulated results for the switch showing aging of the switch for the zeroth, five-hundred thousandth, and one millionth operations. The Young's modulus of the spring material and the coefficient of friction were adjusted in the simulation to match the operation of the switch as it wore. (a) Results recorded from the prototype diverter switch. (b) Simulation results for the diverter switch using the coefficients given in Table II.

D. Endurance Testing

The prototype switch was operated once every 200 ms for 10^6 operations. Fig. 10 compares the data recorded for the zeroth, five-hundred thousandth, and millionth operations to simulation results based on the model given in Section III using the parameters given in Table II. The figure shows that the variation in the operation of the prototype can be replicated in the simulation by varying the operating parameters, especially the spring constant (9) and the contact friction (6), in which case, the simulated results agree well with the actual operation of the

TABLE II
SIMULATION COEFFICIENTS

	<i>Unworn</i>	<i>Partially worn</i>	<i>Worn</i>
No. operations	0	5×10^5	10^6
Coeff. of friction, μ	0.8	1.0	1.8
Young's Modulus, E (GPa)	200	165	130

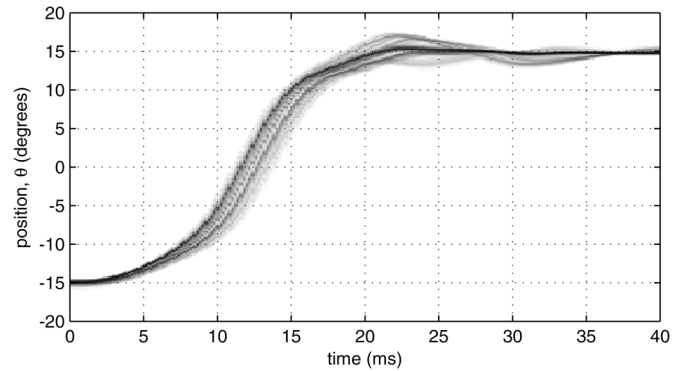


Fig. 11. Density plot compiled from 10^6 operations of the diverter switch showing left to right actuations only.

prototype switch. The simulations suggest that the spring material became less stiff over time, possibly due to fatigue (evident in the slower movement), and that contact friction increased, likely due to roughening of the contact surfaces (evident in the increased damping).

Fig. 11 is a density plot compiled from data for every operation recorded during the trial run. This illustrates how the mechanical performance of the switch varied over the course of the run. The switch consistently operated in under 20 ms (start of motion to opposing contact) although there is some variation in the actuation profile, likely due to weakening of the cantilever springs coupled with an increase in contact friction as indicated by the simulation model.

E. Switch Longevity

After the completion of 10^6 operations, the switch was disassembled to allow examination of the individual components. The nylon parts, including the armature, showed no significant wear. This is a testament to the robustness of the SLS process and the low-energy contact closure scheme that minimized impact impulse forces applied to the system. Notably, the beryllium copper spring layers had begun to show some signs of fatigue in the form of microcracks appearing on the outside (convex) surface. This lends weight to the hypothesis that the

reduction in speed of the switch over the trial run was due primarily to reduced spring stiffness leading to reduced initial accelerating torque.

Photographs of the contact surfaces are shown in Fig. 9. The photographs demonstrate an acceptable level of wear, with no surface indented by more than 0.5 mm. The differences between each set of contacts are fairly small, with only subtly different wear patterns in the contacts subjected to current compared to the no-current contacts. It appears as though the wear rate for both current-carrying contacts is roughly twice that for the mechanical contacts. This is in broad agreement with the wear patterns demonstrated in [1], although it should be noted that the contact material and size of the contacts are very different in these two cases. It is known that sliding contacts of pure copper have relatively poor wear characteristics when compared to harder metals or to noble metals [14]. However, contact resistance and contact temperature are low for a given contact force due to the high ductility and high electrical and thermal conductivities of copper. Coupled with the fact that copper contacts are low cost and that Fig. 9 does not indicate prohibitively high wear rates, it is possible to conclude that copper contacts may be an attractive option for use in a production version of the design.

V. CONCLUSION

Hybrid OLTC systems are one way of tackling distribution network voltage-control problems that will become constraining as EV charging and distributed PV generation become more common. The ability of hybrid OLTC systems to almost completely eliminate electrical arcing during operation allows the mechanical switching system to be drastically reduced in size and mass. This is because the electrical contacts may be designed only to carry the load current, rather than to tolerate arc erosion as in classic OLTC systems. It was hypothesized that this would allow the development of very compact, high-speed air-insulated switching systems capable of operating in under a cycle of the mains waveform. In order to investigate the achievable speed and operation count capability of such a system, a prototype switch was designed, modelled, constructed, and tested. A central design decision was to employ a permanent-magnet actuator to provide high torque with low armature inertia while also generating large static contact forces when unenergized. The results of testing demonstrate good agreement between the model and practice while providing a clear indication of the degradation mechanisms. Crucially, this first prototype delivered more than one million switching operations while also demonstrating very low contact wear rates under realistic electrical contact conditions.

REFERENCES

- [1] D. Rogers and T. Green, "An active-shunt diverter for onload tap changers," *IEEE Trans. Power Del.*, vol. 28, no. 2, pp. 649–657, Apr. 2013.
- [2] R. Tonkoski, D. Turcotte, and T. H. M. El-Fouly, "Impact of high PV penetration on voltage profiles in residential neighborhoods," *IEEE Trans. Sustain. Energy*, vol. 3, no. 3, pp. 518–527, Jul. 2012.

- [3] M. S. Kamarudin, M. Albano, P. Coventry, N. Harid, and A. Haddad, "A survey on the potential of CF3I gas as an alternative for SF6 in high voltage applications," in *Proc. 45th Int. Univ. Power Eng. Conf.*, 2010, pp. 1–5.
- [4] Reinhhausen Group, On-load tap-changers for power transformers, A Technical Digest PB 252/04 Oct. 2010. [Online]. Available: <http://www.reinhhausen.com/>
- [5] H. Jiang, R. Shuttleworth, B. A. Zahawi, X. Tian, and A. Power, "Fast response GTO assisted novel tap changer," *IEEE Trans. Power Del.*, vol. 16, no. 1, pp. 111–115, Jan. 2001.
- [6] Reinhhausen Group, On-load tap-changer vacutap vv, Technical data TD 203/04, Aug. 2010. [Online]. Available: <http://www.reinhhausen.com/>
- [7] P. M. Huang and M. C. Tsai, "Design of a magnet-switching actuator with high efficiency and auto-locking function," *IEEE Trans. Magn.*, vol. 48, no. 11, pp. 4622–4625, Nov. 2012.
- [8] D. J. Rogers, "Hybrid and thin power electronics for electrical power networks," Ph.D. dissertation, Dept. Elect. Comput. Eng., Imperial College London, London, U.K., Feb. 2011.
- [9] K. B. Baltzis, "The FEMM package: A simple, fast, and accurate open source electromagnetic tool in science and engineering," *J. Eng. Sci. Technol. Rev.*, vol. 1, no. 1, pp. 83–89, 2008.
- [10] R. Holm, *Electric Contacts*, 4th ed. Berlin, Germany: Springer-Verlag, 1967.
- [11] S. Timsit, "Electrical contact resistance: Properties of stationary interfaces," in *Proc. 44th IEEE Holm Conf. Elect. Contacts*, Oct. 1998, pp. 1–19.
- [12] B. Goodwine, *Engineering Differential Equations: Theory and Applications*. New York: Springer, 2010.
- [13] P. G. Slade, *Electrical Contacts: Principles and Applications*. New York: Taylor & Francis, 1999, pp. 463–464.
- [14] M. Antler, "Sliding wear of metallic contacts," *IEEE Trans. Compon. Hybrids, Manuf. Technol.*, vol. TCHMT-4, no. 1, pp. 15–29, Mar. 1981.



Daniel J. Rogers (M'11) received the M.Eng. and Ph.D. degrees in electrical and electronic engineering from Imperial College London, London, U.K., in 2007 and 2011, respectively.

Currently, he is a Lecturer in the Institute of Energy, Cardiff University, Cardiff, U.K. He conducts research in collaboration with industry and is involved with the development of high-performance power electronic systems for a variety of companies. He is a co-investigator on the multi-institution EPSRC Energy Storage for Low Carbon Grids project. His interests include the use of medium- and large-scale power-electronic systems to create flexible electrical networks capable of taking advantage of a diverse range of generation technologies, and the subsequent control challenges this produces.



Tim C. Green (M'89–SM'02) received the B.Sc. (Hons.) degree in electrical engineering from Imperial College, London, U.K., in 1986 and the Ph.D. degree in electrical engineering from Heriot-Watt University, Edinburgh, U.K., in 1990.

Currently, he is a Chartered Engineer in the U.K. He was a Lecturer at Heriot Watt University until 1994 and is currently a Professor of Electrical Power Engineering at Imperial College London and Deputy Head of the Electrical and Electronic Engineering Department. His research interest is in formulating

the future form the electricity network to support low-carbon futures. A particular theme is how the flexibility of power electronics and control can be used to accommodate new-generation patterns and new forms of load, such as EV charging, as part of the emerging smart grid. He has particular interests in offshore dc networks and the management of low-voltage networks.

Prof. Green leads the HubNet consortium of eight U.K. universities coordinating research in low-carbon energy networks and is the Network Champion for the Research Councils U.K.



Richard W. Silversides (M'13) received the M.Eng. degree in engineering science from Oxford University, Oxford, U.K., in 1992 and the M.Sc. degree in mechatronics (Hons.) and the Ph.D. degree in engineering from King's College London, London, U.K., in 2002 and 2007, respectively.

He then went to work for the National Grid Company plc, the Transmission Network Owner and Operator for England and Wales, with the Engineering and Technology Group, Leatherhead, U.K., where he achieved Chartered Engineer status. His main inter-

ests were supervisory control and data acquisition and the integration of substation control, monitoring, and protection systems. Currently, he is a Research Associate at Imperial College, London, in the Control and Power Research Group, where he runs the Smart Energy Lab. His research interests are ICT for power networks and power electronics for distribution systems.